

Maskless lithography using silicon oxide etch-stop layer induced by megahertz repetition femtosecond laser pulses

Amirkianoosh Kiani,¹ Krishnan Venkatakrishnan,¹ Bo Tan,^{2,*} and Venkat Venkataraman³

¹Department of Mechanical and Industrial Engineering, Ryerson University, 350 Victoria Street, Toronto, Ontario M5B 2K3, Canada

²Department of Aerospace Engineering, Ryerson University, 350 Victoria Street, Toronto, Ontario M5B 2K3, Canada

³Institute for Optical Sciences, University of Toronto, 60, St. George Street, Suite 331, Toronto, Ontario M5S 1A7, Canada

*tanbo@ryerson.ca

Abstract: In this study we report a new method for maskless lithography fabrication process by a combination of direct silicon oxide etch-stop layer patterning and wet alkaline etching. A thin layer of etch-stop silicon oxide of predetermined pattern was first generated by irradiation with high repetition (MHz) ultrafast (femtosecond) laser pulses in air and at atmospheric pressure. The induced thin layer of silicon oxide is used as an etch stop during etching process in alkaline etchants such as KOH. Our proposed method has the potential to enable low-cost, flexible, high quality patterning for a wide variety of application in the field of micro- and nanotechnology, this technique can be leading to a promising solution for maskless lithography technique. A Scanning Electron Microscope (SEM), optical microscopy, Micro-Raman, Energy Dispersive X-ray (EDX) and X-ray diffraction spectroscopy were used to analyze the silicon oxide layer induced by laser pulses.

©2011 Optical Society of America

OCIS codes: (220.3740) Lithography; (220.4000) Microstructure fabrication; (320.7090) Ultrafast lasers; (350.3850) Materials processing; (350.5340) Photothermal effects.

References and links

1. D. J. Plummer, M. D. Deal, and P. B. Griffin, *Silicon VLSI Technology*, (Englewood Cliffs, NJ: Prentice-Hall, 2000)
2. A. Kiani, K. Venkatakrishnan, and B. Tan, "Micro/nano scale amorphization of silicon by femtosecond laser irradiation," *Opt. Express* **17**(19), 16518–16526 (2009).
3. M. L. Green, E. P. Gusev, R. Degraeve, and E. L. Garfunkel, "Ultrathin (<4 nm) SiO₂ and Si–O–N gate dielectric layers for silicon microelectronics: Understanding the processing, structure, and physical and electrical limits," *J. Appl. Phys.* **90**(5), 2057–2121 (2001).
4. G. Aygun, E. Atanassova, A. Alacakir, L. Ozyuzer, and R. Turan, "Oxidation of Si surface by a pulsed Nd: YAG laser," *J. Phys. D.* **37**(11), 1569–1575 (2004).
5. A. C. R. Grayson, R. S. Shawgo, A. M. Johnson, N. T. Flynn, Y. Li, M. J. Cima, and R. Langer, "A BioMEMS review: MEMS technology for physiologically integrated devices," *Proc. IEEE* **92**(1), 6–21 (2004).
6. G. Saini, R. Gates, M. C. Asplund, S. Blair, S. Attavar, and M. R. Linford, "Directing polyallylamine adsorption on microlens array patterned silicon for microarray fabrication," *Lab Chip* **9**(12), 1789–1796 (2009).
7. D. S. Lee, S. H. Park, H. S. Yang, K. H. Chung, T. H. Yoon, S. J. Kim, K. Kim, and Y. T. Kim, "Bulk-micromachined submicroliter-volume PCR chip with very rapid thermal response and low power consumption," *Lab Chip* **4**(4), 401–407 (2004).
8. A. Kiani, K. Venkatakrishnan, and B. Tan, "Direct patterning of silicon oxide on Si-substrate induced by femtosecond laser," *Opt. Express* **18**(3), 1872–1878 (2010).
9. J. R. Ell, T. A. Crosby, J. J. Peterson, K. R. Carter, and J. J. Watkins, "Formation of SiO₂ air-gap patterns through scCO₂ infusion of NIL patterned PHEMA," *Chem. Mater.* **22**(4), 1445–1451 (2010).
10. G. Della Giustina, M. Guglielmi, G. Brusatin, M. Prascioli, and F. Romanato, "Electron beam writing of epoxy based sol-gel materials," *J. Sol-Gel Sci. Technol.* **48**(1-2), 212–216 (2008).
11. M. Floresarias, A. Castelo, C. Gomezreino, and G. Delafuente, "Phase diffractive optical gratings on glass substrates by laser ablation," *Opt. Commun.* **282**(6), 1175–1178 (2009).

12. K. Aissou, M. Kogelschatz, T. Baron, and P. Gentile, "Self-assembled block polymer templates as high resolution lithographic masks," *Surf. Sci.* **601**(13), 2611–2614 (2007).
13. R. A. Pai, R. Humayun, M. T. Schulberg, A. Sengupta, J. N. Sun, and J. J. Watkins, "Mesoporous silicates prepared using preorganized templates in supercritical fluids," *Science* **303**(5657), 507–510 (2004).
14. D. Yin, S. Horiuchi, and T. Masuoka, "Lateral assembly of metal nanoparticles directed by nanodomain control in block copolymer thin films," *Chem. Mater.* **17**(3), 463–469 (2005).
15. E. J. Carvalho, M. A. R. Alves, E. S. Braga, and L. Cescato, "SiO₂ single layer for reduction of the standing wave effects in the interference lithography of deep photoresist structures on Si," *Microelectron. J.* **37**(11), 1265–1270 (2006).
16. B. Tan, A. Dalili, and K. Venkatakrishnan, "High repetition rate femtosecond laser nano-machining of thin films," *Appl. Phys., A Mater. Sci. Process.* **95**(2), 537–545 (2009).
17. C. F. Guo, S. Cao, P. Jiang, Y. Fang, J. Zhang, Y. Fan, Y. Wang, W. Xu, Z. Zhao, and Q. Liu, "Grayscale photomask fabricated by laser direct writing in metallic nano-films," *Opt. Express* **17**(22), 19981–19987 (2009).
18. K. Venkatakrishnan, B. K. A. Ngoi, P. Stanley, L. E. N. Lim, B. Tan, and N. R. Sivakumar, "Laser writing techniques for photomask fabrication using a femtosecond laser," *Appl. Phys., A Mater. Sci. Process.* **74**(4), 493–496 (2002).
19. H. Yasuda, S. Arai, J. Kai, Y. Ooae, T. Abe, S. Maruyama, and T. Kiuchi, "Multielectron beam blanking aperture array system SYNAPSE-2000," *J. Vac. Sci. Technol. B* **14**(6), 3813–3820 (1996).
20. J. T. Hastings, M. H. Lim, J. G. Goodberlet, and H. I. Smith, "Optical waveguides with apodized sidewall gratings via spatial-phase-locked electron-beam lithography," *J. Vac. Sci. Technol. B* **20**(6), 2753–2757 (2002).
21. J. T. Hastings, F. Zhang, and H. I. Smith, "Nanometer-level stitching in raster-scanning electron-beam lithography using spatial-phase locking," *J. Vac. Sci. Technol. B* **21**(6), 2650–2656 (2003).
22. B. Schmidt, L. Bischoff, and J. Teichert, "Writing FIB implantation and subsequent anisotropic wet chemical etching for fabrication of 3D structures in silicon," *Sens. Actuators A Phys.* **61**(1-3), 369–373 (1997).
23. G. M. Atkinson, F. P. Stratton, R. L. Kubena, and J. C. Wolfe, "30 nm resolution zero proximity lithography on high-Z substrates," *J. Vac. Sci. Technol. B* **10**(6), 3104–3108 (1992).
24. J. P. Spallas, C. S. Silver, and L. P. Muray, "Arrayed miniature electron beam columns for mask making," *J. Vac. Sci. Technol. B* **24**(6), 2892–2896 (2006).
25. M. E. Walsh, and H. I. Smith, "Method for reducing hyperbolic phase in interference lithography," *J. Vac. Sci. Technol. B* **19**(6), 2347–2352 (2001).
26. P. T. Konkola, C. G. Chen, R. K. Heilmann, C. Joo, J. C. Montoya, C. Chang, and M. L. Schattenburg, "Nanometer-level repeatable metrology using the nanoruler," *J. Vac. Sci. Technol. B* **21**(6), 3097–3101 (2003).
27. T. Sandstrom, A. Bleeker, J. Hintersteiner, K. Troost, J. Freyer, and K. van der Mast, "Optical maskless lithography for economic design prototyping and small-volume production," *Proc. SPIE* **5377**, 777–787 (2004).
28. I. W. Moran, A. L. Briseno, S. Loser, and K. R. Carter, "Device fabrication by easy soft imprint nanolithography," *Chem. Mater.* **20**(14), 4595–4601 (2008).
29. S. Krämer, R. R. Fuierer, and C. B. Gorman, "Scanning probe lithography using self-assembled monolayers," *Chem. Rev.* **103**(11), 4367–4418 (2003).
30. J. H. Wei, and D. S. Ginger, "A direct-write single-step positive etch resist for dip-pen nanolithography," *Small* **3**(12), 2034–2037 (2007).
31. F. S. S. Chien, C. L. Wu, Y. C. Chou, T. T. Chen, S. Gwo, and W. F. Hsieh, "Nanomachining of (110)-oriented silicon by scanning probe lithography and anisotropic wet etching," *Appl. Phys. Lett.* **75**(16), 2429–2431 (1999).
32. Y. Y. Zhang, J. Zhang, G. Luo, X. Zhou, G. Y. Xie, T. Zhu, and Z. F. Liu, "Fabrication of silicon-based multilevel nanostructures via scanning probe oxidation and anisotropic wet etching," *Nanotechnology* **16**(4), 422–428 (2005).
33. D. A. Weinberger, S. Hong, C. A. Mirkin, B. W. Wessels, and T. B. Higgins, "Combinatorial generation and analysis of nanometer- and micrometer-scale silicon features via "dip-pen" nanolithography and wet chemical etching," *Adv. Mater.* **12**(21), 1600–1603 (2000).
34. N. Kawasegi, N. Morita, S. Yamada, N. Takano, T. Oyama, and K. Ashida, "Etch stop of silicon surface induced by tribo-nanolithography," *Nanotechnology* **16**(8), 1411–1414 (2005).
35. R. Menon, A. Patel, D. Gil, and H. I. Smith, "Maskless lithography," *Mater. Today* **8**(2), 26–33 (2005).
36. N. Rouhi, B. Esfandyarpour, S. Mohajerzadeh, P. Hashemi, B. Hekmat-Shoar, and M. D. Robertson, "Low temperature high quality growth of silicon-dioxide using oxygenation of hydrogenation-assisted nano-structured silicon thin film," *Mater. Res. Soc. Symp. Proc.* **989**, 95–100 (2007).
37. B. E. Deal, and A. S. Grove, "General relationship for thermal oxidation of silicon," *J. Appl. Phys.* **36**(12), 3770–3778 (1965).
38. J. Blanc, "Revised model for oxidation of Si by oxygen," *Appl. Phys. Lett.* **33**(5), 424–426 (1978).
39. V. K. Samalam, "Theoretical-model for the oxidation of silicon," *Appl. Phys. Lett.* **47**(7), 736–737 (1985).
40. A. Fargeix, and G. Ghibaudo, "Role of stress on the parabolic kinetic constant for dry silicon oxidation," *J. Appl. Phys.* **56**(2), 589–591 (1984).
41. H. Z. Massoud, J. D. Plummer, and E. A. Irene, "Thermal oxidation of silicon in dry oxygen-growth-rate enhancement in the thin regime 0.2. physical-mechanism," *J. Electrochem. Soc.* **132**(11), 2693–2700 (1985).
42. E. G. Gamaly, A. V. Rode, and B. Luther-Davies, "Ultrafast ablation with high-pulse-rate lasers. Part I: Theoretical considerations," *J. Appl. Phys.* **85**(8), 4213–4222 (1999).
43. I. Zergioti, and M. Stuke, "Short pulse UV laser ablation of solid and liquid gallium," *Appl. Phys., A Mater. Sci. Process.* **67**(4), 391–395 (1998).
44. S. Panchatsharam, B. Tan, and K. Venkatakrishnan, "Femtosecond laser-induced shockwave formation on ablated silicon surface," *J. Appl. Phys.* **105**(9), 093103 (2009).

45. J. Bonse, K. W. Brezinka, and A. J. Meixner, "Modifying single-crystalline silicon by femtosecond laser pulses: an analysis by micro Raman spectroscopy, scanning laser microscopy and atomic force microscopy," *Appl. Surf. Sci.* **221**(1–4), 215–230 (2004).
46. A. Y. Vorobyev, and C. L. Guo, "Direct observation of enhanced residual thermal energy coupling to solids in femtosecond laser ablation," *Appl. Phys. Lett.* **86**(1), 011916 (2005).
47. H. R. Shanks, P. D. Maycock, P. H. Sidles, and G. C. Danielson, "Thermal conductivity of silicon from 300 to 1400 degrees K," *Phys. Rev.* **130**(5), 1743–1748 (1963).

1. Introduction

Photolithography is considered to be an important method in a wide range of applications such as fabrication of information storages, micro and nano photonics, nanoelectromechanical systems (NEMS), microelectromechanical systems (MEMS), microfluidics and lab On a Chip Systems [1–7].

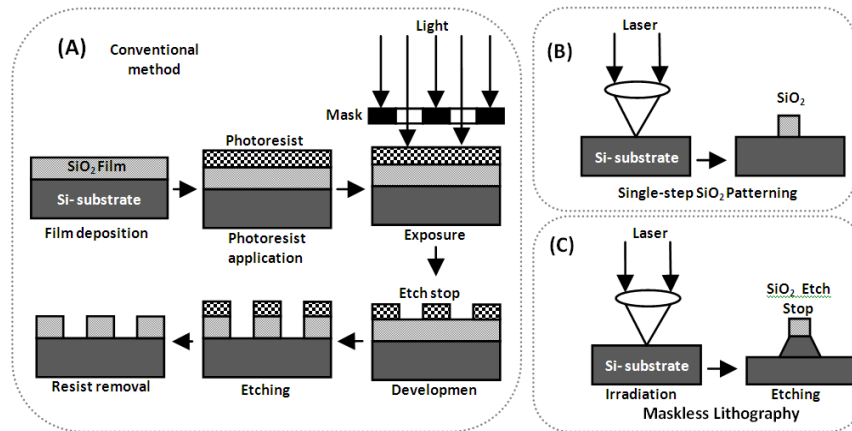


Fig. 1. a) conventional lithography method, b) direct (single-step) silicon oxide patterning, c) direct maskless lithography induced by fs laser.

Patterning layers of etch stop materials on the substrate materials (such as silicon) is one of the most important issues in the photolithography process. Silicon oxide is one of the most attractive materials which is used as an etch stop during etching process. In contrast to other etch stop materials which suffer from one or more problems, silicon oxide offers a lot of desired characteristics and advantages which make silicon oxide an evermore-valuable compound in photolithography method. Known methods for the generation of silicon dioxide (SiO₂) patterns generally involve either physical or chemical vapor deposition; the deposited films must be patterned subsequently using a resist and various etching techniques which are often accomplished through a multi-steps fabrication methods [8–15]. Additionally, conventional photolithography technique is not well-suited to cost-effective, and high-throughput processing since there is several steps in fabrication process and this technique requires photomask for replication which its fabrication is time consuming and expensive [16–18]. Over the past few years, a number of novel techniques such as scanning electron beam lithography (SEBL) [19–21] focused ion-beam (FIB) lithography [22,23], multi-axis electron beam lithography (MAEBL) [24], interference lithography (IL) [25,26] maskless optical projection lithography [27], easy soft imprint nanolithography (ESNIL) [28], scanning-probe and dip pen lithography (SPL, DPL) [29,30], and Tribo Nano Lithography (TNL) based on atomic force microscope (AFM) [31–34] have been reported for maskless replication of micro/nanoscale patterns of silicon oxide on silicon substrate. Although, these techniques have some advantages, they suffer from problems of high cost, low throughput and pattern placement inaccuracy [35]; most of these techniques entail time consuming processing steps and employ complex and expensive equipments which are influenced by environment, also they are only applicable to micron-sized devices and for large scale manufacturing, cell stitch must be performed which can be very challenging due to the small dimension of each

cell. Recently, we reported a new method for generation of oxidized silicon layer on Si substrate by irradiation with fluences below ablation threshold using a high repetition rate femtosecond laser [8]. In this research, we attempt to use this oxidized layer as an etch stop in alkaline etchant, such as KOH to develop a unique approach for single step maskless lithography by a combination of direct-write femtosecond laser oxidation of silicon (etch stop layer) and chemical wet etching. Using a mega hertz frequency femtosecond laser pulses makes it possible to control laser fluence below ablation threshold which causes crystalline silicon conversion to an oxidized silicon. The induced thin layer of oxidized silicon is then used as an etch stop in the following wet chemical etching (KOH) for maskless lithography. In comparison with previous methods, our method can be a promising solution for both direct generation of silicon oxide pattern on Si-substrate (Fig. 1(b)) and maskless lithography (Fig. 1(c)); the direct oxidation of silicon (etch-stop layer) induced by femtosecond laser is a maskless single-step technique which offers a higher flexibility and reduces the processing time. In addition this method allows for the large-area patterning (in mm-scale) at fast writing speed under ambient conditions.

2. Experimental setup

To study the direct patterning of silicon oxide, undoped <100> oriented silicon wafers were used. Prior to laser irradiation, silicon samples were rinsed in an acetone and then treated in a pure water. First, silicon wafers were irradiated of predetermined pattern with fs pulses with pulse energy controlled in oxidation range under ambient conditions. In order to investigate the feasibility of using this technique in applications such as lithography, the irradiated samples were etched in a KOH solution.

The Femtosecond laser used in the study was a diode-pumped, Yb-doped system. This laser emits pulses of 214 fs pulse duration. Using a harmonic generator, the laser beam is converted to the second harmonic (515) central wavelength. The theoretical diameter of the focused laser spot is calculated to be 5.2 μm [2]. Samples were irradiated with laser beams of power of 3.3 W at pulse frequency of 26 MHz and a speed of scanning of 100 mm/s (laser intensity, $I = 0.15 \text{ J/cm}^2$). Irradiated samples were observed and analyzed using a scanning electron microscopy (SEM), an optical microscopy, a Micro-Raman, an Energy Dispersive X-ray (EDX) and a X-ray diffraction spectroscopy.

3. Results and discussion

Figure 2 shows morphology of the oxidized silicon patterns on Si-substrate after irradiation with sub-ablation threshold femtosecond laser pulses. SEM images show bump lines around 7 μm width and 500 nm height induced with femtosecond laser pulses with a power of 3.3 W supplied at 26 MHz. As shown in Fig. 2, the embossed lines (made of silicon oxide) can be generated consistently on a silicon surface with carefully controlled laser parameters.

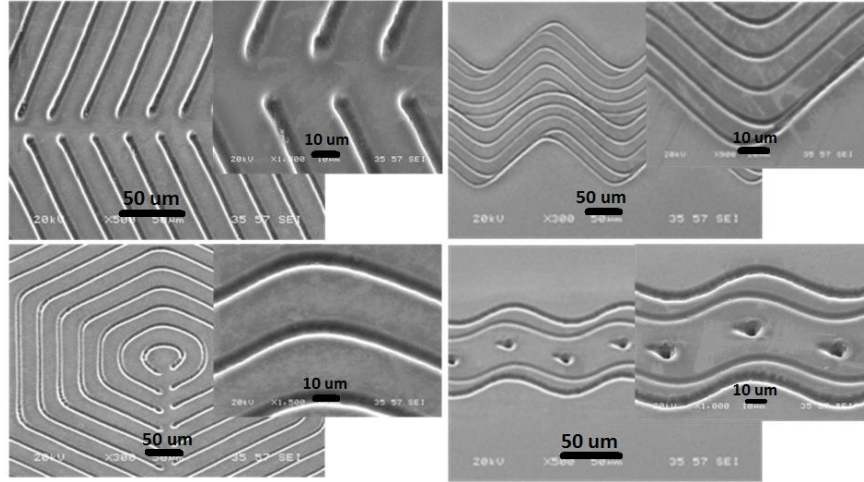


Fig. 2. SEM images of silicon oxide pattern induced by 214 fs laser pulses at the frequency of 26 MHz and the average power of 3.3 W ($I = 0.15 \text{ J/cm}^2$).

Generally in the silicon oxidation process, the final silicon oxide layer is approximately 54% above and 46% below the original silicon surface which is because of the difference in densities between Si and SiO_2 [36]. Figure 3(a) represents optical microscope topography images of the induced areas after irradiation. Cross sectional views show embossed lines around 500 nm high and 7 μm width induced at the laser power of 3.3 W and frequency of 26 MHz with the pulse duration of 214 fs. Due to this fact that the final oxide layer is 54% above and 46% below the original surface, it can be concluded that the real thickness of oxide layer on Si-substrate is approximately 1 μm .

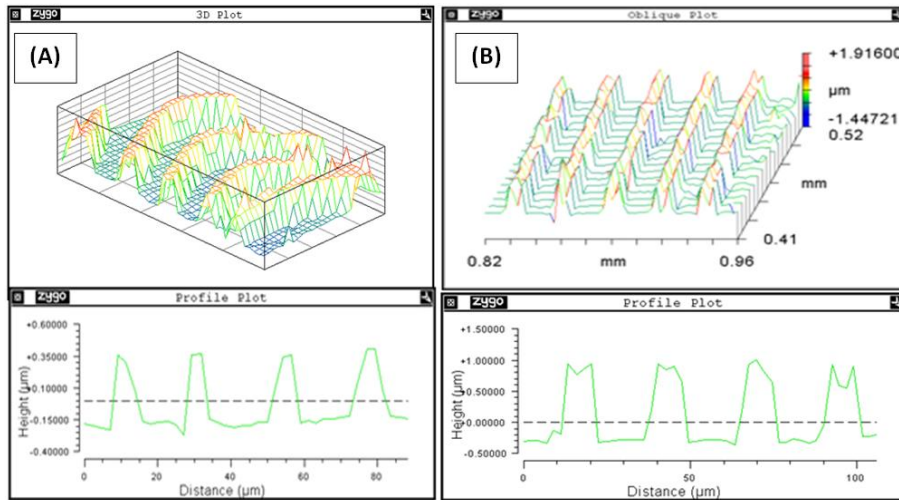


Fig. 3. Optical microscope topography and cross sectional images (a) after irradiation (height: 500nm) and (b) after etching process (height: 1000 nm).

In order to verify the elemental composition of the irradiated area (embossed lines), EDX and Raman spectroscopic analyses were hired. EDX results indicated the existence of oxygen in irradiated lines which are explained to be due to the Si-O-Si bounds in an irradiated area (Fig. 4).

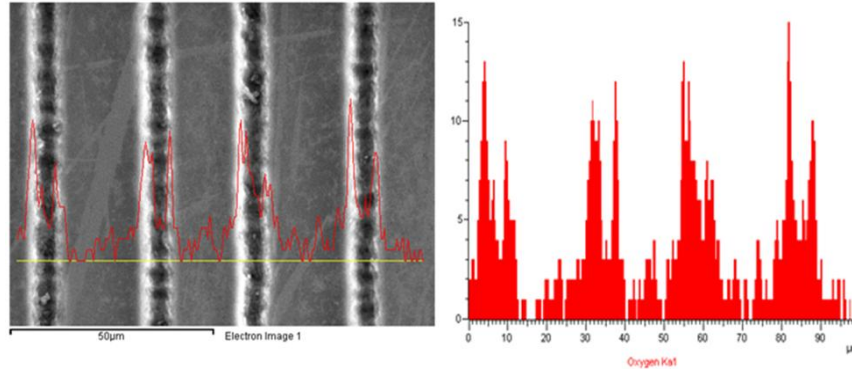


Fig. 4. EDX results of irradiated area.

Raman spectroscopy was dominated by the signal at wavenumber of 519 cm^{-1} which is the characteristic peak of silicon (Fig. 5). Also, a hump was observed at the wavenumber of 954 cm^{-1} corresponding to silicon oxide [37]. Back scattering micro-Raman analysis was performed under ambient conditions using 532 nm line of Ar ion laser source. Consequently, it can be concluded that irradiated lines were converted to silicon oxide.

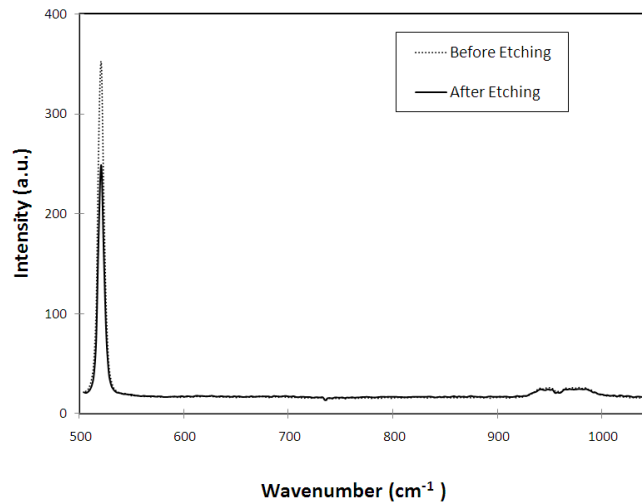


Fig. 5. micro-Raman spectroscopy results of irradiated samples before/after etching process.

Figure 6 shows X-ray diffractometer (XRD) data for the silicon samples before and after irradiation by laser. XRD measurement of the samples was performed using a X-ray diffractometer equipped with the X-ray source of Cu rotating anode generator ($\lambda = 1.54184\text{Å}$) operated in a large angle rate of 10° - 60° . In spite of the good resolution of XRD measurements, the spectra of laser irradiated samples (post-irradiation) exhibits only one crystalline peak in the spectra of laser irradiated sample and no other crystalline peaks of Si were detected. Also, the XRD graph of the laser treated samples (post-irradiation) shifted to the lower level of intensity. Therefore, it can be concluded that the irradiated area converted from a crystalline silicon to an amorphous silicon oxide (a-SiO_x) which is in agreement with other spectroscopy results obtained by micro-Raman and EDX.

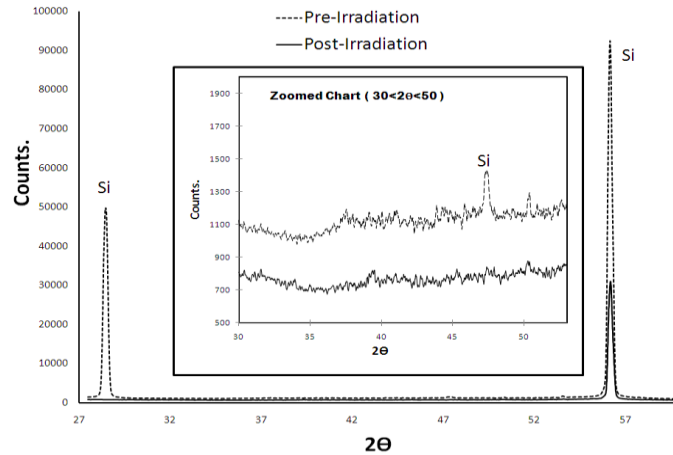


Fig. 6. XRD results of pre/post-irradiated samples. XRD spectrum of pre-irradiated area is dominated by the signals at $2\theta = 28, 56$ and 47 (zoomed chart) which corresponds to crystalline silicon. The XRD measurements on the processed samples shows only a peak shifted to lower level of intensity at $2\theta = 56$.

The manufacture of many micro/nano scale devices from silicon requires the use of an etch stop layer to selectively stop the anisotropic etching of silicon at the chemical etchant such as KOH. Previous studies proposed by researchers have shown that the silicon oxide is an excellent material for creating etch-stop layers on the silicon wafers. Figure 7, shows SEM images of the induced samples after etching in a 30% KOH alkaline solution at temperature of 65°C after 4 minutes. As shown, the silicon oxidized pattern on silicon substrate acted as an etch stop during the etching process and finally micro scale features were generated on the silicon substrate. Figure 3(b) shows optical microscope topography images of induced Si samples after etching in KOH. As shown in cross sectional view, the height of the generated lines after etching is around $1\ \mu\text{m}$ supporting the fact that bumps are made of silicon oxide and act as an etch stop in an alkaline etchant.

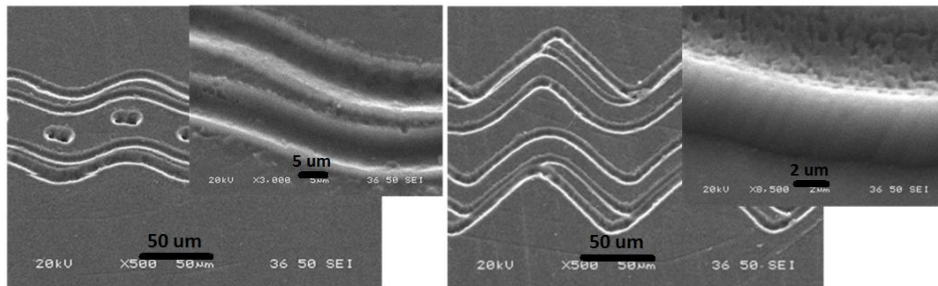


Fig. 7. SEM images of silicon oxide pattern after etching in KOH (30%) at 65°C after 5 min.

Figure 5 shows the micro-Raman spectroscopy results of the irradiated lines before and after the etching process. The peak at $520\ \text{cm}^{-1}$ which is corresponding of crystalline silicon shifted to a lower energy level after an etching but the peak of silicon oxide remained nearly in the same level of energy supporting this statement that the irradiated area converted to a silicon oxide and acted as an etch stop during the etching process in KOH.

The growth of an oxide layer can be modeled by a number of well-known thermal models such as Deal-Grove model [38]. During the last years, some laser induced models have been proposed by researchers, it can be concluded from the proposed simulations based on thermal models that oxidation of silicon occurs at the temperature in the range of $1000\sim 1600\ \text{K}$ [8,38–41].

Using high repetition (MHz) ultrafast (fs) laser pulses enable us to bring the temperature of the target surface to the oxidation temperature range and keep it in this range. In other words, the laser fluence can be controlled to be below the ablation threshold and in the oxidation range by using the megahertz frequency femtosecond laser irradiation.

As indicated by [16,42,43], if it is assumed that the laser energy is absorbed in a layer much thinner than the penetration depth of the heat wave, thus the one-dimensional heat conduction equation can be calculated by:

$$\frac{\partial T}{\partial t} = a \frac{\partial^2 T}{\partial x^2}, \quad (1)$$

where $a = k/C_p\rho_0$, a is thermal diffusion, k is the heat conduction and C_p is specific heat and finally, ρ_0 is irradiated material density. In order to simplify, it is assumed that the profile of laser pulse is in a rectangular shape with the step-like rise and fall [43], thus:

$$T(x,t) = k\sqrt{\frac{a}{\pi}} \int_0^{t_p} \frac{I_a(\tau)}{\sqrt{t-\tau}} \exp\left\{-\frac{x^2}{2a(t-\tau)}\right\} d\tau. \quad (2)$$

The maximum surface temperature, T_{max} , takes place at the end of the laser pulse, i.e. $T_{max} = T(0, t_p)$, where t_p is pulse duration; thus the surface temperature at the center of spot area during the laser pulse ($t < t_p$) can be calculated by $T(t) = \sqrt{t/t_p} T_{max}$. Using the same conduction equation, the surface temperature after the end of the pulse at the center of the spot area can be calculated as:

$$T(0,t) = T(0,t_p) \left(\frac{t_p}{t}\right)^{1/2} = \sqrt{\frac{2}{\pi}} \frac{I_a(at_p)^{1/2}}{k} \left(\frac{t_p}{t}\right)^{1/2}, \quad (3)$$

where, I_a is the absorbed laser light intensity which is estimated by [44]:

$$I_a = \frac{4PK(1-R)}{\pi d^2 t_p f}. \quad (4)$$

Here, K is residual energy coefficient, R is reflection coefficient, P is average power, f is frequency and d is spot diameter. Combining two previous equations and simplifying:

$$T_{max} = T(0, t_p) = \sqrt{\frac{2a}{\pi^3 t_p}} \frac{4K(1-R)P}{kfd^2}. \quad (5)$$

T_{max} is the maximum temperature at the end of the pulse and T_{min} is the minimum temperature at the beginning of the next laser pulse which is given by $T_{min} = \alpha T_{max}$. Where α is equal to $\alpha = \sqrt{t_p/t_{pp}}$ (t_{pp} is pulse interval and given by $t_{pp} = 1/f$). The maximum and minimum surface temperatures after n pulses can be approximately calculated as:

$$(T_{max})_n = (1 + \alpha + \alpha^2 + \alpha^3 + \dots + \alpha^{n-1})T_m = \left[\frac{1-\alpha^n}{1-\alpha}\right]T_m, \quad (6)$$

$$(T_{min})_n = \alpha(T_{max})_n.$$

The average surface temperature after n pulses is calculated with:

$$\bar{T}_n = \frac{1}{n(t_p + t_{pp})} \int_0^{n(t_p + t_{pp})} T(0,t) dt = 2\alpha \frac{(1-\frac{2}{3}\alpha)T_m}{(1+\alpha^2)(1-\alpha)} \left(1 + \frac{\alpha^n - \alpha}{n(1-\alpha)}\right). \quad (7)$$

According to [45], R , the reflection coefficient of silicon during irradiation by femtosecond laser pulses is 0.393 and 0.329 at the wavelength of 488 nm and 800 nm, respectively. Thus, the reflection coefficient of silicon can be calculated to be around 0.38 at 520 nm. In the case of below ablation laser fluence, the residual energy coefficient for silicon, K , is 0.8 [46]; thermal conductivity, k , is 155 W/mK and thermal diffusivity is $8.5 \times 10^{-5} \text{ m}^2/\text{s}$ [47]. The effective number of pulses in our experiment was calculated to be around 1700 by $N_{eff} = \sqrt{\pi/2} fd/v$, where v is scanning speed (100 mm/s).

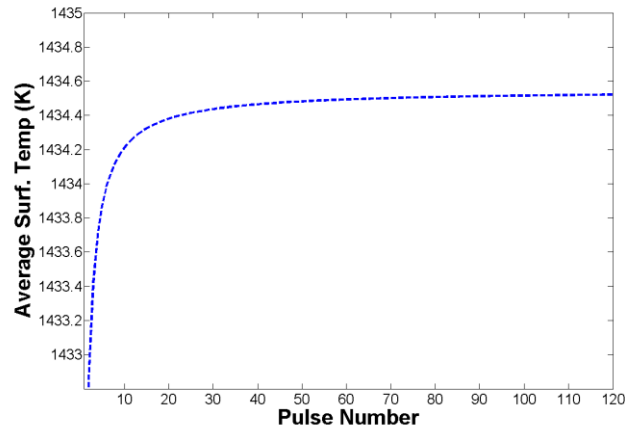


Fig. 8. Computed results for average surface temperature vs. number of pulses ($f = 26 \text{ MHz}$, $t_{pp} = 214 \text{ fs}$, $P = 3.3 \text{ W}$).

The computed results in Fig. 8, show that initially the surface temperature increases with the accumulation of number of pulses ($N < 20$). However further increase in pulse number causes the average surface temperature reaches saturation. The final surface temperature at 26 MHz at the power of 3.3 W is around 1434 °K which falls in into the temperature range (1000-1600 °K) and can lead to generation of the silicon oxide on the substrate surface of the crystalline silicon wafer. In fact, increased number of pulses (more than 30) will not lead to the heat accumulation and ablation on a silicon substrate since the silicon substrate cools off between pulses no matter how many pulses are applied into the target.

4. Conclusion

In this study, we proposed a new method for direct patterning of silicon oxide etch-stop layer on a silicon substrate using high repetition ultrafast laser pulses which enable us to control the laser fluence and the target surface temperature below the ablation threshold and keep the surface temperature in the oxidation temperature range. This technique is potentially useful for a single-step patterning of etch-stop layer of silicon oxide on a Si surface for a wide variety of applications in MEMS, NEMS and Lab On a Chip (LOC) devices fabrication. The oxidized silicon pattern can be used as an etch stop in the etching process for fabrication of micro/nano scale features. In comparison with previous maskless methods, this technique offers a higher flexibility and reduced processing time and cost of fabrication. This technique does not require a photomask and any redesign can be easily done in the large scanning fields (mm × mm) by using CAD software for the beam scanning.

Acknowledgments

This research is funded by the Natural Science and Engineering Research Council of Canada and the Ministry of Research and Innovation, Ontario.